Article

Quadrupolar, Highly Polarized Dyes: Emission Dependence on Viscosity and Selective Mitochondria Staining

Mariusz Tasior, Olena Vakuliuk, Antoni Wrzosek, Valentine I. Vullev,* Adam Szewczyk,* Denis Jacquemin,* and Daniel T. Gryko*

Read Online

ACCESS | ull Metrics & More | Article Recommendations | SI Supporting Information

ABSTRACT: Quadrupolar A-D-A-type 1,4-dihydropyrrolo[3,2-b]pyrroles (DHPPs) bearing pyridinium and quinolinium substituents emit in the 500−600 nm region. The enhancement of electronic communication between the electron-rich heterocyclic core and electron-deficient peripheral substituents turned out to be crucial for achieving emission enhancement in viscous media. DHPP bearing two 4-pyridinium substituents has optical brightness 34,000 in glycerol and only 700 in MeOH, as evidenced by measurements of the emission intensity and fluorescence lifetimes in a series of polar solvents. Such behavior makes it an excellent candidate for viscosity probes in fluorescence microscopy, as demonstrated by the fluorescence imaging of H9C2 cardiomyocytes.

In methanol $\Phi_{fl} = 0.0086$

In glycerol $\Phi_{fl} = 0.48$ $\lambda_{em} = 515$ nm

2TfO⁻
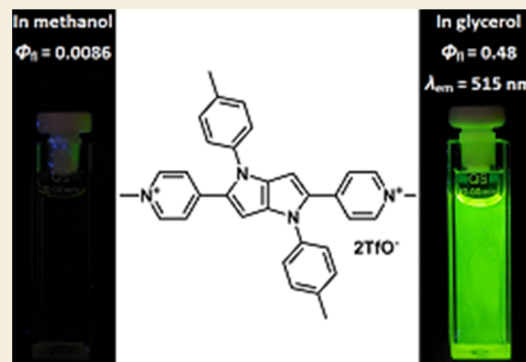
KEYWORDS: dyes/pigments, fluorescence, heterocycles, donor−acceptor systems, viscosity

Changes in microenvironment-related parameters such as viscosity, polarity, and pH play important roles in biological systems. An abnormal internal microenvironment may lead to cellular malfunction and the occurrence of various diseases.[1] In particular, the anomalous viscosity behavior of cells is often accompanied by dramatic changes in the levels of biologically relevant analytes, including reactive oxygen species and signal molecules. Therefore, in the last few decades, remarkable advances have been made toward the development of viscosity-sensitive fluorescent probes.[2−4] These probes are particularly efficient for imaging viscosity in biomembranes and are additionally useful for targeting specific organelles, such as mitochondria and lysosome. Tracking of the viscosity parameter in these organelles is important because its perturbations are associated with many diseases, including Parkinson's, Huntington's, Alzheimer's, cardiovascular diseases, as well as diabetes.[5−7] A common structural motif in viscosity-sensitive fluorescent probes is a molecular rotor composed of an electron donor and electron acceptor. The hindering of rotor rotation in a viscous environment leads to the deactivation of one of the fluorescence quenching pathways and, consequently, to a significant increase in the emission intensity. In this type of sensor, a pyridinium cation is often the electron acceptor. Due to the fact that it is charged, it also significantly increases the solubility of the probe in the aqueous environment.

We hypothesized that centrosymmetric, quadrupolar, and dicationic dyes should form a new class of small molecular fluorescent probes for imaging of viscosity. For designing such

dyes, we considered several candidates for an electron-rich scaffold, but we eventually chosen 1,4-dihydropyrrolo[3,2-b]pyrrole (DHPP) due to the following reasons: (1) exceptionally high-lying highest occupied molecular orbital (HOMO); (2) straightforward and modular synthesis; (3) possibility of vast structural modification. Their chemistry was hampered for many years by the lack of an efficient synthetic methodology;[8] however, this situation changed dramatically in 2013, when we serendipitously found a method that allows quick access to 1,4-dihydro-tetraarylpyrrolo[3,2-b]pyrroles (TAPPs).[9−11] This multicomponent reaction involves the formation of a Schiff base and subsequent condensation with diacetyl in an acidic medium. We recently developed improved conditions for this reaction, which now allow the preparation of TAPPs on the multigram scale in good yields.[12] The better access to these compounds is reflected by their use in a growing number of applications in research related to their photophysics,[13] excited-state symmetry breaking (ES-SB),[14−17] direct solvent probing via H-bonding interactions,[18] conjugated polymers,[19] organic field-effect transistors,[20] bulk heterojunction organic solar cells,[21] organic light-emitting

diodes,[22] dye-sensitized solar cells,[23] resistive memory devices,[24] aggregation-induced emission,[25−28] and metal−organic frameworks (MOFs).[29] TAPPs are also an excellent platform for the synthesis of the π-expanded heteroanalogues of polycyclic aromatic hydrocarbons.[30−39] In this publication, we present our efforts to test the above-mentioned hypothesis.

DESIGN AND SYNTHESIS

Recent studies on the photophysical properties of 1,4-dihydro-tetraarylpyrrolo[3,2-b]pyrroles revealed that only substituents at positions 2 and 5 of the DHPP core have a major impact on their photophysical properties.[12,15−17] The influence of substituents at positions 1 and 4 is much weaker; therefore, aryl groups installed at those positions could be used to tune further properties, such as solubility in organic solvents, if desired. We anticipated that the synthesis of TAPPs with heterocyclic quaternary salts as substituents at positions 2 and 5 should lead to quadrupolar A-D-A-type dyes in which these substituents play a dual role: a strong electron acceptor and solubilizing group in an aqueous environment. We resolved to insert both pyridinium and quinolinium substituents differing in position of quaternary ammonium salt versus DHPP core. Anticipating that the type of charged heterocyclic subunit can play a vital role in determining photophysical response, we also designed dyes with five-membered rings, i.e., thiazolium and benzothiazolium moieties. In fact, 2,5-bispyridyl-1,4-dihydropyrrolo[3,2-b]pyrroles were already prepared multiple times usually using older, less efficient catalysts.[40,41] With a good methodology that puts pyridine-bearing pyrrolo[3,2-b]pyrroles in our hands,[10] we synthesized a series of these dyes 4a−g with substituents at positions 2 and 5 that differ in heteroarene size and bridging position (Scheme 1, Figure 1). TAPPs 4a−g were subsequently alkylated using methyl triflate in N,N-dimethylformamide (DMF), affording the final dyes 5a−g in just two steps, with a good overall yield and without the need for any excessive purification except for evaporation of reaction mixtures and subsequent crystallization from an appropriate solvent. All prepared compounds were bench stable, had yellow to orange color, and were insoluble in nonpolar solvents.

SPECTROSCOPIC PROPERTIES

The photophysical properties of all prepared dyes 5a−g were studied in solvents of similar polarity but dramatically different viscosities, namely, methanol, ethylene glycol, and glycerol. For comparison with conventional solvents, the absorption and emission of 5a−g were also measured in sucrose octaacetate (SOA), which is known to form room-temperature glass. Methylation of the heteroaryl substituents leads to dyes whose absorption and emission maxima are bathochromically shifted (416−512 nm region) relative to the parent TAPPs, which typically absorb at ca. 360−380 nm (Table 1, Figures 2, S1−S35). This red shift was expected due to the significant change in acceptor character of the substituents at positions 2 and 5 from electron-neutral/weakly accepting to strongly electron-withdrawing, inducing strong charge transfer (CT), a fact confirmed by computational studies (see below). This red shift is slightly weaker for compounds 5b, 5e, 5f, and 5g having two methylated nitrogen atoms in position 2 of the heteroaryl substituent, which can be explained by the weaker ground-state electronic coupling between the core and side moieties for steric reasons.

Scheme 1. Synthesis of 1,4-Dihydropyrrolo[3,2-b]pyrroles Bearing Pyridinium/Thiazolium Substituents
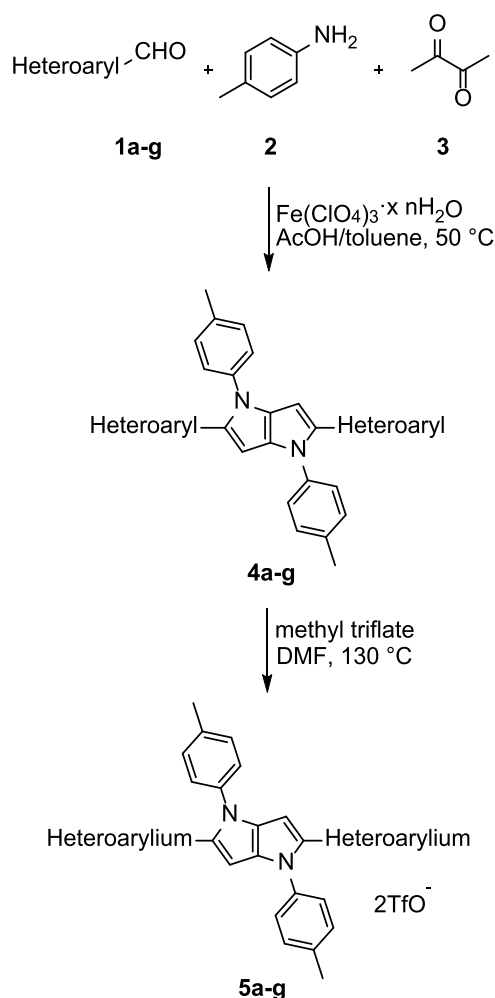
π-Expansion of peripheral substituents at positions 2 and 5 without altering the position of charged nitrogen atoms (pyridinium → quinolinium, 5a → 5c) results in a ca. 50 nm bathochromic shift of absorption and almost 100 nm shift of emission. The larger shift of emission corresponds to larger changes in the corresponding dihedral angles between the ground and excited states (vide infra). An analogous, although slightly different, effect was observed upon comparison of 5b and 5e, both possessing a nitrogen atom in the vicinity of the DHPP core. Steric hindrance imposed by methyl groups is plausibly responsible for the hypsochromic shift of absorption of 5b vs 5a (≈50 nm). At the same time, emission is bathochromically shifted, which corresponds to a significant Stokes shift (almost 7000 cm⁻¹) in MeOH. When comparing 5b and 5e, one can notice a bathochromic shift of absorption and emission, which is, however, much smaller compared to 5a → 5c. According to expectations, moving the quaternary nitrogen atom to a less conjugated position (5c → 5d) causes a small hypsochromic shift of absorption and a 100 nm shift of emission (Table 1). This results from weaker quadrupolar A-D-A coupling since acceptor moieties have less interaction with the central donor. Compared to TAPPs possessing naphthalen-1-yl substituents at positions 2 and 5,[43] dye 5c has significantly (by ca. 150 nm) red-shifted absorption maxima. TAPPs possessing five-membered thiazolium rings (or in the case of
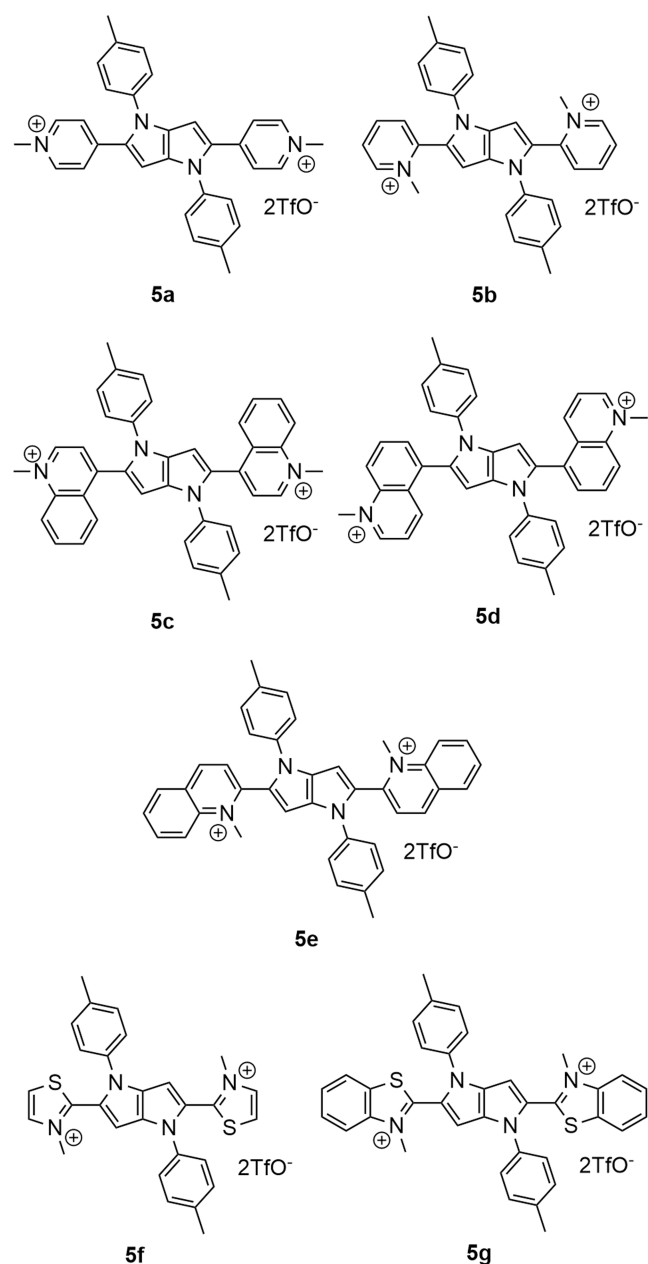
Figure 1. Structures of the final dyes.

5g, benzothiazolium ones) have hypsochromically shifted absorption and emission (as well as stronger emission) versus dyes **5a**–**5e** (Table 1). Data for TAPP **5a** strictly corresponds to the published data for this dye.[41]

Due to the similar polarity of the tested solvents, negligible differences in the absorption maxima between solutions of individual compounds are observed. Similarly, the emission wavelength of the tested compounds is not strongly affected by changing the solvent, except for dye **5b**. Such a significant ca. 60 nm difference in emission maxima on **5b** is very likely caused by much faster relaxation in the excited state in methanol, while in glycerol, the electronic transition is faster than molecular motion; thus, the emission takes place from a geometry close to the Franck–Condon one. Importantly, as we anticipated, most of the tested dyes exhibit significant emission enhancement upon exposure to highly viscous environments. This effect was particularly strong for dyes **5a**–**5c**, for which an

over 50-fold increase in the fluorescence quantum yield was observed. Use of the solid medium (SOA) resulted in the same fluorescence enhancement. Also, the fluorescence intensity of **5a** and **5b** in a water–glycerol mixed solvent system increased as the glycerol content increased, that is, as the viscosity increased (Figures S36–S39). On the other hand, dye **5d** remained nonfluorescent even in highly viscous solvents, while compound **5g** emits relatively strongly in all tested solvents, and we used theory to help rationalizing these trends (*vide infra*). Having planned biological tests, we also checked the properties of new dyes in the aqueous environment (50 mM sodium phosphate buffer (PBS), pH = 7.4). They were practically copies of those measured in methanol. At the tested 10^{-7}–10^{-6} M concentration range, we did not observe any signs of aggregation (with perfect linearity of absorbance and emission intensity with respect to the concentration), which could be expected from large aromatic dyes.

THEORETICAL MODELING

We used density-functional theory (DFT) and time-dependent DFT (TD)-DFT to model all synthesized dyes, the medium (methanol) effects being treated with an approach including both *linear-response* and *state-specific* corrections, cLR²,[43] which is well-suited in the case of bright CT dyes. No structural simplification was made, but the counterions were neglected in the calculations. For all compounds, theory finds a bright lowest excited state with the expected A-D-A topology. This can be clearly seen in Figure 3, where the electron density difference (EDD) plots are given for all molecules: one notes that the DHPP moiety appears in blue, indicating that it loses density upon excitation, whereas the pyridinium/quinolinium side groups are in red, indicating that they gain density. In other words, photon absorption induces a strong CT transition from DHPP core towards the lateral groups. Interestingly, for all dyes, TD-DFT optimization returns no indication of ES-SB, as the structures are true minima of the excited-state potential energy surface in the C_i point group.

To allow for direct comparisons between the measured and computed values, we provide in Table 2 a summary of key computed data, and especially the 0–0 energies,[44] that pave the way for well-grounded theory–experiment comparisons. Illustratively for **5a** and **5g**, theory provides 2.69 and 2.77 eV, slightly blue-shifted as compared to the experimental value of 2.52 and 2.61 eV. The 0.1–0.2 eV difference is typical of this level of theory, but importantly one notices that the trends in 0–0 energies given by theory parallel their experimental counterparts but for **5b**, in which the much red-shifted emission is not reproduced by the calculations. The same holds for the vertical absorption wavelengths: they qualitatively follow their experimental counterparts with a determination coefficient of 0.99 between experimental and theoretical absorption energies. Interestingly, the rather limited red-shift in going from **5f** to **5g** (exp: +24 nm, theory: +28 nm) can be explained by the EDDs of Figure 3, as the contribution of the extra benzene rings added to the electron-withdrawing groups is obviously modest.

In Table 2, we also provide the dihedral angles between the TAPP core and the side pyridinium/quinolinium rings for both the optimized ground- and excited-state geometries. As can be seen, there is a systematic planarization of the dyes in the excited state, which is the expected trend in such quadrupolar CT systems.[13,15,42] However, both the absolute values of the dihedral angles and their actual fluctuations upon change of

Table 1. Spectroscopic Properties of Dyes 5a−g Measured in Different Solvents

compound	solvent	λ_{abs}^{max} [nm]	ε_{max} [M^{-1} cm^{-1}]	λ_{em}^{max} [nm]	Φ_{fl}	τ_{fl} [ps]	Stokes shift $\Delta\lambda$ [cm^{-1}]
5a	methanol	470	76 800	518	0.0086[a]	n.d.	1970
	ethylene glycol	470	70 900	517	0.088[a]	n.d.	1930
	glycerol	472	70 100	515	0.48[a]	673, 1600	1770
	SOA	469		517	0.70[a]	2700	1980
	PBS	464	58 600	519	0.0033[a]	n.d.	2280
5b	methanol	415	27 000	582	0.00085[b]	n.d.	6910
	ethylene glycol	414	26 100	553	0.0036[b]	n.d.	6070
	glycerol	416	22 900	525	0.044[b]	323, 810	4990
	SOA	416		497	0.33[b]	1600, 4100	3920
	PBS	410	24 300			n.d.	
5c	methanol	522	39 800			306	
	ethylene glycol	522	32 600	611	0.0066[c]	450	2790
	glycerol	527	27 300	605	0.10[c]	300, 926	2450
	SOA	524		610	0.11[c]	1300, 3700	2690
	PBS	514	30 500				
5d	methanol	508	11 700			541, 5300	
	ethylene glycol	506	10 600			772, 6200	
	glycerol	509	8700			976, 6700	
	SOA	503					
	PBS	483	8600				
5e	methanol	484	49 500			925	
	ethylene glycol	485	46 800	579	0.01[a]	2600	3350
	glycerol	488	42 700	573	0.11[a]	268, 883, 1800	3040
	SOA	489		573	0.11[a]	1800, 3300	3000
	PBS	479	29 700				
5f	methanol	416	39 400	480	0.035[b]	270	3210
	ethylene glycol	419	36 900	482	0.10[b]	658	3120
	glycerol	422	26 500	479	0.18[b]	785, 1100	2820
	SOA	419		482	0.39[b]	868, 1400	3120
	PBS	415	41 400	480	0.0085[b]	n.d.	3260
5g	methanol	441	58 500	513	0.08[a]	511	3180
	ethylene glycol	454	59 300	517	0.29[a]	346, 912	2680
	glycerol	456	57 400	511	0.30[a]	619, 1100	2360
	SOA	443		509	0.09[a]	766, 1700	2930
	PBS	450	32 000	511	0.09[a]	n.d.	2650

[a]Measured with fluorescein in ethanol ($\Phi = 0.79$) as reference. [b]Measured with coumarin 153 in ethanol ($\Phi = 0.38$) as reference. [c]Measured with fluorescein in NaOH (0.1 M) ($\Phi = 0.91$) as reference.

electronic state depend on the actual structure, with planarization going from ca. −7° (**5a**) to ca. −21° (**5f**) in the present series.

Eventually, we realized relaxed TD-DFT scans of the excited-state potential energy surfaces for both the rotation of the pyridinium/quinolinium moieties and the rotation of the tolyl groups (attached to the nitrogen atoms) around the DHPP core. Interestingly, we found rotation barriers in a rather tight range around ca. 10 kcal·mol^{-1}, which is a value reasonably average (not too small, not too large) to be significantly affected by the solvent viscosity. In more detail, the barrier for the full "flipping" of the charged side group in the excited state goes from 7.9 (**5d**) to 13.6 (**5a** and **5g**) kcal·mol^{-1}. In contrast, for the rotation of the N-linked tolyl group, the values go from 8.7 (**5d**) to 11.6 (**5g**) kcal·mol^{-1}. It is interesting to see that **5d** has the smallest barriers of the whole series for both rotation, which is consistent with it being the least emissive dye of the series, likely due to effective nonradiative deactivation through a "fan effect." Even viscous solvents seem to be unable to counter this effect. In contrast, **5g** enjoys the largest barriers, for both pyridinium and tolyl moieties, and is experimentally the most emissive dye in

methanol: the rotation barriers are large enough to allow significant emission even in the least viscous solvent.

■ BIOLOGICAL STUDIES

Among the tested dyes, the spectroscopic behavior of compounds **5a−5c** was particularly interesting because of the 50-fold fluorescence quantum yield enhancement in viscous solvents. This effect is especially desired in fluorescent probes intended for reporting changes in cell microenvironments as it secures low background noise and high brightness in fluorescence microscopy. With the goal of proving the usefulness of these new dyes, we performed studies on the localization of compounds **5a**, **5b**, and **5d** in cells. Dye **5a** was a particularly promising candidate for viscosity probe, as it is practically nonfluorescent in methanol, while its fluorescence quantum yield reaches almost 50% in glycerol. Dye **5b** is less fluorescent in glycerol and was selected for biological tests because it represents one of the two synthesized dyes that possess an ortho substituent. Dye **5d**, on the other hand, is not emissive even in a glassy matrix.

The stability tests showed that most promising dyes **5a** and **5b** are perfectly stable in the PBS buffer during 48 h of storage
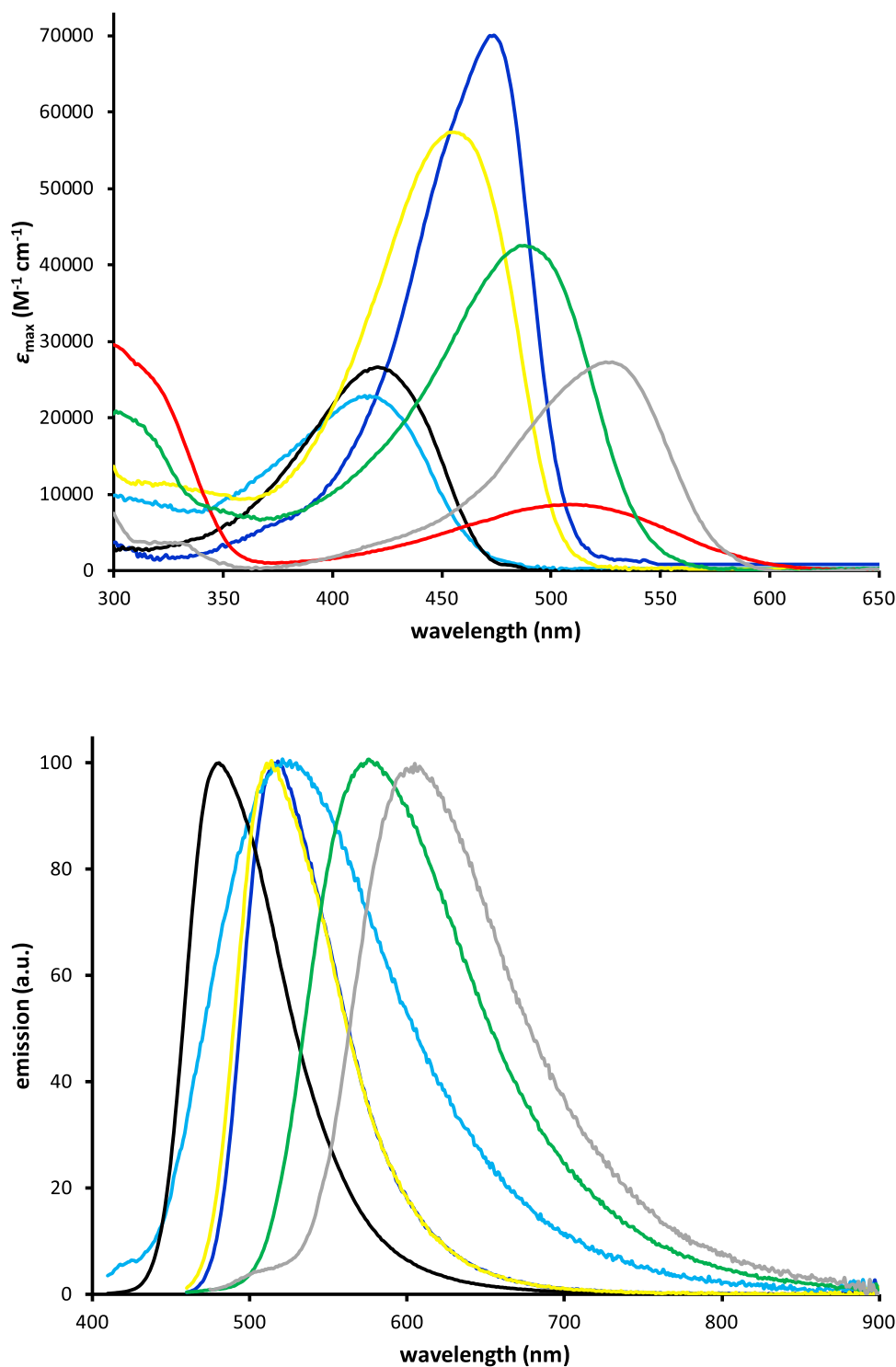
Figure 2. Absorption (top panel) and normalized fluorescence spectra (bottom panel) of **5a** (blue line), **5b** (light blue line), **5c** (gray line), **5d** (red line), **5e** (green line), **5f** (black line), and **5g** (yellow line) measured in glycerol.

in darkness (Figures S40−S41). Incubation of cells with our cationic dyes for 16 h showed that only **5a** could be localized in the mitochondria of H9C2 cells using fluorescence microscopy (Figure 4). The staining of mitochondria was confirmed by the colocalization with mitochondrial marker Mito Red (Figure 4). The Pearson's *R* value was 0.79, Meanders' M1 was 0.979, and M2 was 0.975. When a single magnified cell was used for measurements (Figure 4B), the Pearson's *R* value was 0.86, Meanders' M1 was 0.973, and M2

was 0.963. This means that the colocalization of **5a** in the cell was similar to that of the well-established mitochondrial marker Mito Red. When the mitochondrial uncoupling compound FCCP was added 1 μM after incubation of the cells with **5a** and Mito Red, the fluorescence of **5a** remained almost unchanged. We can conclude that both the entry of the compound into cells and the labeling of cells are fairly slow processes, but also its efflux from the mitochondria is limited after the transmembrane potential of the inner mitochondrial
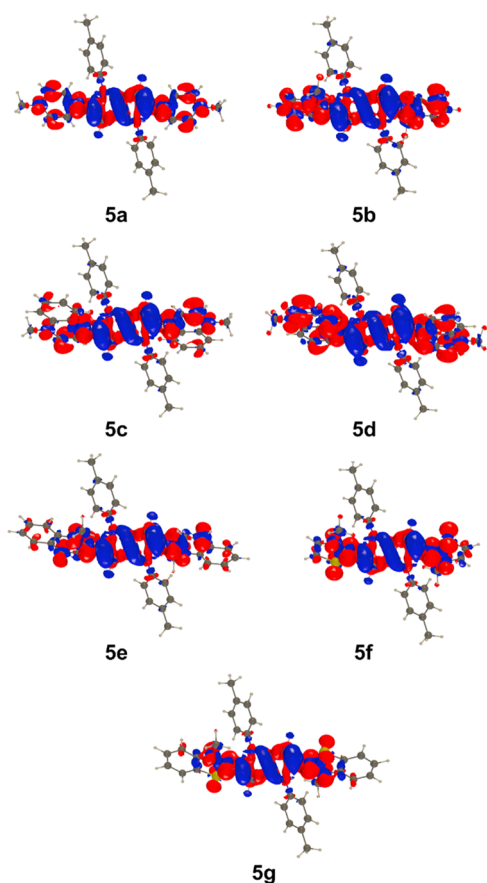
Figure 3. Density difference representation of the lowest excited states. Blue and red regions, respectively, correspond to decrease and increase of density upon absorption. Contour: 0.001 au.

Table 2. Key TD-DFT Results for 5a−g in MeOH: Vertical Absorption and Emission Wavelengths, 0−0 Energies, and Dihedral Angle between the DHPP Core and Heteroaryllium as Computed in the Ground and Excited States

compound	$\lambda^{vert-abs}$ [nm]	$\lambda^{vert-fl}$ [nm]	E^{0-0} [eV]	$\phi^{ground-state}$ [deg.]	$\phi^{excited-state}$ [deg.]
5a	415	500	2.69	26.5	19.1
5b	366	471	3.01	54.8	34.9
5c	457	567	2.44	45.2	35.8
5d	455	621	2.29	51.0	39.0
5e	422	528	2.63	48.9	34.6
5f	362	478	2.97	49.1	28.2
5g	390	507	2.77	45.7	26.9

membrane is substantially reduced (Figure 4C). The other two compounds localized in the cell in amounts undetectable by the detector amplifications used for compound **5a** and below detection of autofluorescence of the cell (Figure S1A,B). The compounds **5a**, **5b**, and **5d** used in the study were not toxic to H9C2 cells as demonstrated by the Orangu test (Figure 5). The slight increase in absorbance was due to the presence of Pluronic F 127 and DMSO rather than the compounds used in the studies (Figure S43).

To obtain information about the binding mode of our cationic dyes to mitochondria, we performed experiments involving spectrophotometric and spectrofluorimetric titration of the dye **5a** solution in PBS using plasmid DNA and bovine
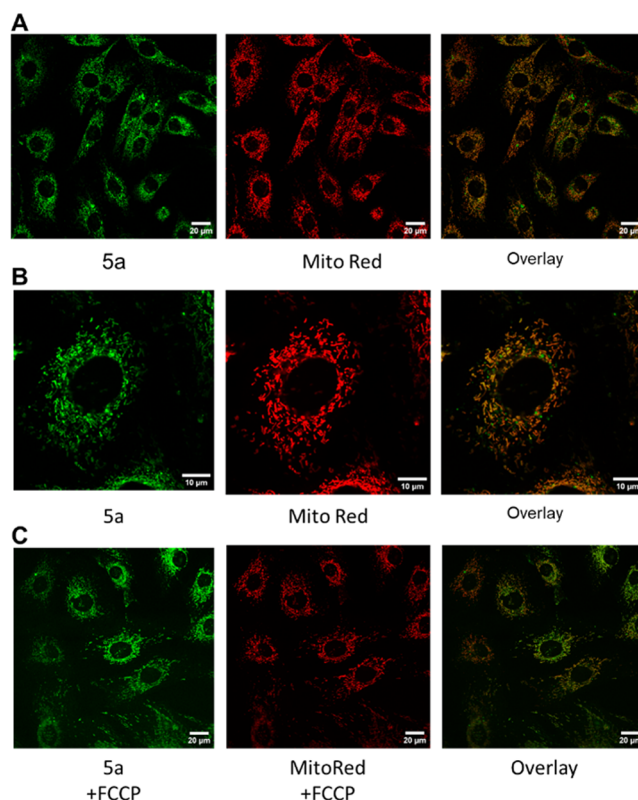

Figure 4. Intracellular localization of **5a** as detected using confocal fluorescence microscopy. (A) The fluorescence of **5a** was recorded with a 473 nm excitation wavelength, and fluorescence of Mito Red was recorded with a 559 nm excitation wavelength. Overlay picture recorded simultaneously for two fluorophores in living H9C2 cells. (B) Pictures for selected cells from above regions were recorded with higher magnification (3x) for a better resolution. (C) Changes of fluorescence intensity of the **5a** dye in Mito Red after treating the cells with mitochondrial uncoupler FCCP for 30 min. The concentration of the **5a** compound was 0.5 μM.
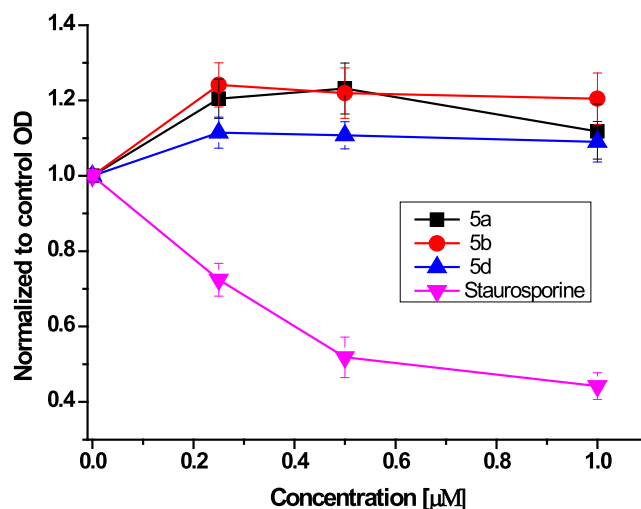

Figure 5. Toxicological test of compounds **5a** (squares), **5b** (circles), and **5d** (triangles) using Orangu test. As a positive control, staurosporine (inverted triangles) was used, a well-known compound that in the micromolar range caused necrosis and apoptosis of the cells. The Orangu test was conducted after the 16 h incubation of the cells with compounds. The bars represent standard error of the mean (SEM).

serum albumin (BSA). Although the addition of DNA increases the fluorescence intensity of the dye, indicating its binding, this effect is approximately 7-fold weaker than that of Hoechst 33342 dye used as a control, taking the same dye/nucleic acid ratio (Figures S44–S47). The absorbance of TAPP **5a** does not change significantly upon binding to DNA. Titration with BSA also shows a fluorescence enhancement, presumably as a result of binding of the dye to the multiple pockets present in this transport protein. However, significant changes (more than 2-fold) in fluorescence are visible only when the protein concentration is at least 6 times higher than the concentration of the analyzed dye. Therefore, it can be cautiously concluded that dye binding by DNA and proteins does not have a crucial impact on the observed spectroscopic behavior of the dye inside the cell, and microenvironmental factors might play a major role in this regard.

■ CONCLUSIONS

In conclusion, we successfully synthesized a library of water-soluble dicationic A-D-A-type dyes composed of the pyrrolo[3,2-*b*]pyrrole scaffold as a central motif decorated with pyridinium/thiazolium moieties. In some cases, the resulting dyes exhibit significant fluorescence enhancement in viscous solvents. Critically, the fluorogenic response is controlled by both the type of charged electron-deficient heterocycle and the bridging position. Computational investigations enabled us to postulate that fluorescence enhancement in viscous media is correlated with rotation barrier of rings carrying quaternary salts.

Biological tests showed that only dye possessing 4-pyridinium moieties (**5a**) could be localized and revealed fluorescence in mitochondria of the H9C2 cells. One particularly interesting feature of compound **5a** was that it accumulated in the cell relatively slowly within hours, which can be used in fluorescence microscopy in the context of observing long-term changes in the mitochondrial network in living cells. No effect on the survival of H9C2 cells, even at relatively high concentrations as for the compound accumulated in mitochondria, and no staining of other cellular structures were observed, which makes it a good marker for long-term observations of changes in the mitochondrial network.

■ EXPERIMENTAL SECTION

General Information

All chemicals were used as received unless otherwise noted. All reported NMR spectra were recorded on a 500 MHz spectrometer, unless otherwise noted. Chemical shifts (δ; ppm) for ^{1}H and ^{13}C NMR were determined with tetramethylsilane (TMS) as the internal reference. *J* values are given in Hz. Mass spectra were obtained with an EI ion source and the EBE double focusing geometry mass analyzer or spectrometer equipped with an electrospray ion source with a Q-TOF type mass analyzer.

The DFT and TD-DFT calculations were performed with Gaussian 16. For all dyes, the real structures were used, but the counterions have been neglected. Default Gaussian 16 thresholds and algorithms were used, but for an improved optimization threshold (10^{-5} au on average residual forces), a stricter self-consistent field convergence criterion (10^{-10} a.u.) and the *ultrafine* DFT integration grid were used. All further details are given in the Supporting Information.

The rat embryonic cardiomyoblast-derived H9C2 cell line was used in biological studies. The cells cultured at 37 °C in a humidified atmosphere containing 5% CO_2 in DMEM supplemented with 10% fetal bovine serum, 2 mM glutamine, 100 U/mL of penicillin, and 100

μg/mL of streptomycin to reach 80% of confluence. In order to determine the viability of cells under the influence of the tested compounds, an Orangu test was performed. Staurosporine was used as a positive control for cell death. Hoechst 33342 in DMSO (ThermoFischer, H21492; 10 mg/mL) and a Plasmid Miniprep DNA Purification Kit (EURx Ltd. Gdansk, Poland, E3500) were used for DNA-binding studies. Bovine serum albumin (BSA, Sigma, A7030) was used in the albumin-binding studies. All further details are given in the Supporting Information.

General Procedure for the Synthesis of Pyrrolo[3,2-*b*]pyrroles 4a–g

Glacial acetic acid (4.5 mL), toluene (4.5 mL), aldehyde (6 mmol), and *p*-toluidine (642 mg, 6 mmol) were placed in a 25 mL round-bottom flask equipped with a magnetic stir bar. The mixture was immersed in a preheated to 50 °C well-stirred oil bath and stirred for 1 h. After that, Fe(ClO$_4$)$_3$·xH$_2$O (63 mg) was added, followed by diacetyl (0.26 mL, 4 mmol). The resulting mixture was stirred at 50 °C in an open flask under air overnight. Solvents were removed using a rotary evaporator; 10 mL of toluene was added and evaporated again to ensure the removal of traces of acetic acid. The resulting dark brown mixture was boiled with 15 mL of acetonitrile for 30 s. After the mixture was cooled down, the precipitate was filtered off, washed with cold acetonitrile, and dried under vacuum.

1,4-Bis(4-methylphenyl)-2,5-bis(pyridin-4-yl)-1,4-dihydro-pyrrolo-[3,2-*b*]pyrrole (4a). Yellow solid. Yield: 0.28 g (21%). Spectral and optical properties concur with literature data.[12]

1,4-Bis(4-methylphenyl)-2,5-bis(pyridin-2-yl)-1,4-dihydro-pyrrolo-[3,2-*b*]pyrrole (4b). Yellow solid. Yield: 0.25 g (19%). Spectral and optical properties concur with literature data.[12]

1,4-Bis(4-methylphenyl)-2,5-bis(quinolin-4-yl)-1,4-dihydro-pyrrolo-[3,2-*b*]pyrrole (4c). Brown solid. Yield: 0.47 g (28%). ^{1}H NMR (500 MHz, CDCl$_3$): δ = 8.73 (d, *J* = 4.5 Hz, 2H), 8.34 (d, *J* = 8.5 Hz, 2H), 8.13 (d, *J* = 8.5 Hz, 2H), 7.70 (t, *J* = 7.0 Hz, 2H), 7.49 (t, *J* = 7.0 Hz, 2H), 7.15–7.05 (m, 10H), 6.66 (s, 2H), 2.30 (s, 6H) ppm. ^{13}C{^{1}H} NMR (126 MHz, CDCl$_3$): δ = 149.3, 148.8, 139.6, 136.6, 135.8, 132.2, 131.4, 129.9, 129.6, 129.4, 126.8, 126.7, 126.4, 124.3, 122.3, 98.5, 20.9 ppm. HRMS (EI): *m/z* calculated for C$_{38}$H$_{28}$N$_4$: 540.2314 [M$^{·+}$]; found 540.2303.

1,4-Bis(4-methylphenyl)-2,5-bis(quinolin-5-yl)-1,4-dihydro-pyrrolo-[3,2-*b*]pyrrole (4d). Brown solid. Yield: 0.50 g (31%). ^{1}H NMR (500 MHz, CDCl$_3$): δ = 8.86 (d, *J* = 2.5 Hz, 2H), 8.51 (d, *J* = 8.5 Hz, 2H), 8.05 (d, *J* = 8.5 Hz, 2H), 7.63 (t, *J* = 8.0 Hz, 2H), 7.44 (d, *J* = 7.0 Hz, 2H), 7.31–7.27 (m, 2H), 7.06 (d, *J* = 8.5 Hz, 4H), 6.98 (d, *J* = 8.5 Hz, 4H), 6.52 (s, 2H), 2.24 (s, 6H) ppm. ^{13}C{^{1}H} NMR (126 MHz, CDCl$_3$): δ = 150.2, 148.4, 137.0, 135.2, 134.9, 132.1, 131.0, 130.7, 129.7, 129.1, 128.8, 127.5, 124.0, 121.0, 97.1, 20.9 ppm. HRMS (EI): *m/z* calculated for C$_{38}$H$_{28}$N$_4$: 540.2314 [M$^{·+}$]; found 540.2316.

1,4-Bis(4-methylphenyl)-2,5-bis(quinolin-2-yl)-1,4-dihydro-pyrrolo-[3,2-*b*]pyrrole (4e). Brown solid. Yield: 0.98 g (60%). ^{1}H NMR (500 MHz, CDCl$_3$): δ = 7.98 (d, *J* = 8.5 Hz, 2H), 7.94 (d, *J* = 9.0 Hz, 2H), 7.73 (d, *J* = 8.5 Hz, 2H), 7.69 (t, *J* = 7.5 Hz, 2H), 7.49 (d, *J* = 7.5 Hz, 2H), 7.23–7.13 (m, 10H), 6.91 (s, 2H), 2.38 (s, 6H) ppm. ^{13}C{^{1}H} NMR (126 MHz, CDCl$_3$): δ = 151.7, 147.3, 137.0, 136.4, 136.3, 136.2, 130.2, 130.0, 129.0, 128.2, 127.661, 127.5, 127.53, 126.5, 126.3, 125.3, 124.9, 123.1, 121.8, 120.9, 97.7, 20.9 ppm. HRMS (EI): *m/z* calculated for C$_{38}$H$_{28}$N$_4$: 540.2314 [M$^{·+}$]; found 540.2301.

1,4-Bis(4-methylphenyl)-2,5-bis(thiazol-2-yl)-1,4-dihydro-pyrrolo-[3,2-*b*]pyrrole (4f). Yellow solid. Yield: 0.47 g (34%). Spectral and optical properties concur with literature data.[43]

2,5-Bis(benzothiazol-2-yl)-1,4-bis(4-methylphenyl)-1,4-di-hydropyrrolo-[3,2-*b*]pyrrole (4g). Brown solid. Yield: 0.98 g (60%). ^{1}H NMR (500 MHz, CDCl$_3$): δ = 7.90 (d, *J* = 8.0 Hz, 2H), 7.70 (d, *J* = 8.0 Hz, 2H), 7.41–7.38 (m, 6H), 7.31 (d, *J* = 8.0 Hz, 4H), 7.27–7.24 (m, 2H), 6.98 (s, 2H), 2.49 (s, 6H) ppm. ^{13}C{^{1}H} NMR (126 MHz, CDCl$_3$): δ = 159.1, 138.1, 135.8, 134.9, 134.8, 132.7, 130.0, 127.2, 126.1, 124.5, 122.5, 121.1, 97.0, 21.3 ppm. HRMS (EI): *m/z* calculated for C$_{34}$H$_{22}$N$_4$S$_2$: 552.1442 [M$^{·+}$]; found 552.1449.

General Procedure for the Synthesis of Pyridinium/Thiazolium Pyrrolo[3,2-b]pyrroles 5a−g

Pyrrolo[3,2-b]pyrrole (0.5 mmol) was dissolved in dry DMF (10 mL). Next, MeOTf (230 μL, 2.1 mmol, **ATTENTION: toxic**) was added. The resulting mixture was immersed in a preheated 130 °C well-stirred oil bath and stirred for 16 h. After cooling down, solvent was removed using a rotary evaporator, and the residue was triturated with dichloromethane (DCM). Yellow-to-orange precipitate was filtered off, washed with DCM, and dried under vacuum.

4,4′-(1,4-Di-p-tolyl-1,4-dihydropyrrolo[3,2-b]pyrrole-2,5-diyl)bis(1-methylpyridin-1-ium) Bis-(trifluoromethanesulfonate) (5a). Orange solid. Yield: 0.34 g (83%). ^{1}H NMR (500 MHz, DMSO-d_6): δ = 8.64 (d, J = 7.0 Hz, 4H), 7.69 (d, J = 7.0 Hz, 4H), 7.39 (d, J = 8.0 Hz, 4H), 7.33 (d, J = 8.0 Hz, 4H), 7.30 (s, 2H), 4.13 (s, 6H), 2.41 (s, 6H) ppm. ^{13}C{^{1}H} NMR (126 MHz, DMSO-d_6): δ = 146.0, 144.9, 138.2, 137.5, 135.7, 134.5, 131.2, 126.1, 123.2, 121.1 (q, J = 328 Hz), 101.2, 47.1, 21.1 ppm. ^{19}F NMR (470 MHz, DMSO-d_6): δ = −77.8 ppm. HRMS (ESI): m/z calculated for $C_{32}H_{30}N_4$: 235.1230 [M-2TfO$^-$]$^{2+}$; found 235.1235.

2,2′-(1,4-Di-p-tolyl-1,4-dihydropyrrolo[3,2-b]pyrrole-2,5-diyl)bis(1-methylpyridin-1-ium) Bis-(trifluoromethanesulfonate) (5b). Yellow solid. Yield: 0.32 g (82%). ^{1}H NMR (500 MHz, DMSO-d_6): δ = 9.08 (d, J = 6.0 Hz, 2H), 8.39 (t, J = 8.0 Hz, 2H), 8.00 (t, J = 8.0 Hz, 2H), 7.72 (td, J = 7.0, 1.0 Hz, 2H), 7.26 (s, 8H), 7.21 (s, 2H), 4.36 (s, 6H), 2.32 (s, 6H) ppm. ^{13}C{^{1}H} NMR (126 MHz, DMSO-d_6): δ = 147.8, 147.0, 144.6, 137.5, 135.0, 133.1, 131.5, 131.0, 126.8, 126.5, 125.0, 121.1 (q, J = 324 Hz), 101.1, 47.9, 20.9 ppm. ^{19}F NMR (470 MHz, DMSO-d_6): δ = −77.8 ppm. HRMS (ESI): m/z calculated for $C_{32}H_{30}N_4$: 235.1230 [M-2TfO$^-$]$^{2+}$; found 235.1238.

4,4′-(1,4-Di-p-tolyl-1,4-dihydropyrrolo[3,2-b]pyrrole-2,5-diyl)bis(1-methylquinolin-1-ium) Bis-(trifluoromethanesulfonate) (5c). Red-brown solid. Yield: 0.26 g (60%). ^{1}H NMR (500 MHz, DMSO-d_6): δ = 9.19 (d, J = 6.0 Hz, 2H), 8.64 (d, J = 8.5 Hz, 2H), 8.44 (d, J = 8.5 Hz, 2H), 8.23 (t, J = 8.0, 2H), 7.94 (t, J = 8.0 Hz, 2H), 7.63 (d, J = 6.5 Hz, 2H), 7.27 (d, J = 8.0 Hz, 4H), 7.20 (d, J = 8.0 Hz, 4H), 7.14 (s, 2H), 4.50 (s, 6H), 2.28 (s, 6H) ppm. ^{13}C{^{1}H} NMR (126 MHz, DMSO-d_6): δ = 148.2, 147.7, 139.5, 137.0, 136.0, 135.6, 135.5, 132.6, 130.9, 130.4, 129.4, 126.7, 125.2, 121.9, 121.1 (q, J = 324 Hz), 119.8, 103.1, 45.4, 20.9 ppm. ^{19}F NMR (470 MHz, DMSO-d_6): δ = −77.8 ppm. HRMS (ESI): m/z calculated for $C_{40}H_{34}N_4$: 285.1386 [M-2TfO$^-$]$^{2+}$; found 285.1393.

5,5′-(1,4-Di-p-tolyl-1,4-dihydropyrrolo[3,2-b]pyrrole-2,5-diyl)bis(1-methylquinolin-1-ium) Bis-(trifluoromethanesulfonate) (5d). Orange solid. Yield: 0.34 g (77%). ^{1}H NMR (500 MHz, DMSO-d_6): δ = 9.43 (d, J = 5.5 Hz, 2H), 9.30 (d, J = 8.5 Hz, 2H), 8.41 (d, J = 9.0 Hz, 2H), 8.18 (t, J = 8.0, 2H), 8.02 (d, J = 8.5, 5.5 Hz, 2H), 7.78 (d, J = 7.5 Hz, 2H), 7.14 (d, J = 7.5 Hz, 4H), 7.10 (d, J = 7.5 Hz, 4H), 6.71 (s, 2H), 4.63 (s, 6H), 2.22 (s, 6H) ppm. ^{13}C{^{1}H} NMR (126 MHz, DMSO-d_6): δ = 150.6, 146.0, 139.4, 136.3, 136.2, 134.9, 133.7, 132.4, 132.1, 131.0, 130.5, 128.4, 125.0, 123.6 (q, J = 324 Hz), 122.5, 118.5, 99.4, 46.3, 20.9 ppm. ^{19}F NMR (470 MHz, DMSO-d_6): δ = −77.8 ppm. HRMS (ESI): m/z calculated for $C_{40}H_{34}N_4$: 285.1386 [M-2TfO$^-$]$^{2+}$; found 285.1397.

2,2′-(1,4-Di-p-tolyl-1,4-dihydropyrrolo[3,2-b]pyrrole-2,5-diyl)bis(1-methylquinolin-1-ium) Bis-(trifluoromethanesulfonate) (5e). Orange solid. Yield: 0.38 g (86%). ^{1}H NMR (500 MHz, DMSO-d_6): δ = 8.94 (d, J = 7.0 Hz, 2H), 8.55 (d, J = 7.5 Hz, 2H), 8.35 (d, J = 6.5 Hz, 2H), 8.27 (t, J = 6.5, 2H), 8.02 (t, J = 6.5 Hz, 2H), 7.74 (d, J = 7.0 Hz, 2H), 7.44 (s, 2H), 7.36 (d, J = 7.0 Hz, 4H), 7.27 (d, J = 7.0 Hz, 4H), 4.64 (s, 6H), 2.32 (s, 6H) ppm. ^{13}C{^{1}H} NMR (126 MHz, DMSO-d_6): δ = 150.7, 144.5, 140.3, 137.7, 136.2, 135.0, 134.7, 131.1, 130.7, 130.3, 129.7, 128.1, 126.0, 125.0, 121.1 (q, J = 324 Hz), 120.3, 103.7, 43.9, 21.0 ppm. ^{19}F NMR (470 MHz, DMSO-d_6): δ = −77.8 ppm. HRMS (ESI): m/z calculated for $C_{40}H_{34}N_4$: 285.1386 [M-2TfO$^-$]$^{2+}$; found 285.1397.

2,2′-(1,4-Di-p-tolyl-1,4-dihydropyrrolo[3,2-b]pyrrole-2,5-diyl)bis(3-methylthiazol-3-ium) Bis-(trifluoromethanesulfonate) (5f). Yellow solid. Yield: 0.39 g (100%). ^{1}H NMR (500 MHz, DMSO-d_6): δ = 8.43 (d, J = 4.0 Hz, 2H), 8.16 (d, J = 4.0 Hz, 2H), 7.45 (d, J = 8.0 Hz, 4H), 7.39 (d, J = 8.0 Hz, 4H), 7.29 (s, 2H), 4.12 (s, 6H), 2.40 (s, 6H) ppm. ^{13}C{^{1}H} NMR (126 MHz, DMSO-d_6): 159.6, 139.2, 139.1, 135.3, 133.4, 131.2, 126.9, 124.9, 124.6, 121.1 δ = (q, J = 324 Hz), 101.2, 41.2, 21.1 ppm. ^{19}F NMR (470 MHz, DMSO-d_6): δ = −77.8 ppm. HRMS (ESI): m/z calculated for $C_{28}H_{26}N_4S_2$: 241.0794 [M-2TfO$^-$]$^{2+}$; found 241.0802.

2,2′-(1,4-Di-p-tolyl-1,4-dihydropyrrolo[3,2-b]pyrrole-2,5-diyl)bis(3-methylbenzothiazol-3-ium) Bis-(trifluoromethanesulfonate) (5g). Orange solid. Yield: 0.44 g (100%). ^{1}H NMR (500 MHz, DMSO-d_6): δ = 8.36 (t, J = 6.0 Hz, 4H), 7.93−7.90 (m, 2H), 7.79−7.76 (m, 2H), 7.58 (d, J = 7.0 Hz, 4H), 7.49 (s, 2H), 7.41 (d, J = 7.0 Hz, 4H), 4.41 (s, 6H), 2.40 (s, 6H) ppm. ^{13}C{^{1}H} NMR (126 MHz, DMSO-d_6): 162.7, 141.9, 139.3, 136.6, 133.9, 131.3, 130.3, 130.2, 129.0, 126.7, 125.9, 124.9, 121.1 (q, J = 324 Hz), 117.9, 103.7, 54.9, 21.1 ppm. ^{19}F NMR (470 MHz, DMSO-d_6): δ = −77.8 ppm. HRMS (ESI): m/z calculated for $C_{36}H_{30}N_4S_2$: 291.0951 [M-2TfO$^-$]$^{2+}$; found 291.0961.

■ ASSOCIATED CONTENT

Data Availability Statement

The data underlying this study are available in the published article and its Supporting Information.

Ⓢ Supporting Information

The Supporting Information is available free of charge at https://pubs.acs.org/doi/10.1021/acsorginorgau.3c00035.

> It contains materials, methods, experimental details, UV details, and characterization data (^{1}H, ^{13}C NMR, and ^{19}F NMR spectra of all isolated compounds) (PDF)

■ AUTHOR INFORMATION

Corresponding Authors

Valentine I. Vullev − Department of Bioengineering, University of California, Riverside, California 92521, United States; Department of Chemistry, University of California, Riverside, California 92521, United States; Department of Biochemistry and Materials Science and Engineering Program, University of California, Riverside, California 92521, United States; ⓞ orcid.org/0000-0002-3416-9686; Email: vullev@ucr.edu

Adam Szewczyk − Nencki Institute of Experimental Biology of Polish Academy of Sciences, 02-093 Warsaw, Poland; Email: a.szewczyk@nencki.gov.pl

Denis Jacquemin − Nantes Université, CNRS, CEISAM, F-44000 Nantes, France; Institut Universitaire de France (IUF), F-75005 Paris, France; ⓞ orcid.org/0000-0002-4217-0708; Email: Denis.Jacquemin@univ-nantes.fr

Daniel T. Gryko − Institute of Organic Chemistry, Polish Academy of Sciences, 01-224 Warsaw, Poland; ⓞ orcid.org/0000-0002-2146-1282; Email: dtgryko@icho.edu.pl

Authors

Mariusz Tasior − Institute of Organic Chemistry, Polish Academy of Sciences, 01-224 Warsaw, Poland

Olena Vakuliuk − Institute of Organic Chemistry, Polish Academy of Sciences, 01-224 Warsaw, Poland

Antoni Wrzosek − Nencki Institute of Experimental Biology of Polish Academy of Sciences, 02-093 Warsaw, Poland

Complete contact information is available at:

https://pubs.acs.org/10.1021/acsorginorgau.3c00035

Author Contributions

M.T. conceived the idea and wrote the manuscript. M.T. and O.V. performed all synthetic and spectroscopic experiments. A.W. and A.S. performed biological studies and wrote the analysis. V.I.V. supervised the spectroscopic studies. D.J. performed DFT and TD-DFT calculations, analyzed data, and wrote and reviewed the manuscript. D.T.G. supervised the project, performed formal analysis, and wrote and reviewed the manuscript. All the authors discussed the results and commented on the manuscript. CRediT: **Mariusz Tasior** conceptualization, investigation, writing-original draft, writing-review & editing; **Olena Vakuliuk** investigation, writing-original draft; **Antoni Wrzosek** investigation, visualization, writing-original draft; **Valentine I. Vullev** supervision, writing-review & editing; **Adam Szewczyk** writing-original draft, writing-review & editing; **Denis Jacquemin** investigation, visualization, writing-original draft, writing-review & editing; **Daniel T. Gryko** supervision, writing-original draft, writing-review & editing.

Notes

The authors declare no competing financial interest.

■ REFERENCES

(1) Luby-Phelps, K. Cytoarchitecture and Physical Properties of Cytoplasm: Volume, Viscosity, Diffusion, Intracellular Surface Area. *Int. Rev. Cytol.* **1999**, *192*, 189−221.

(2) Ma, C.; Sun, W.; Xu, L.; Qian, Y.; Dai, J.; Zhong, G.; Hou, Y.; Liua, J.; Shen, B. A Minireview of Viscosity-Sensitive Fluorescent Probes: Design and Biological Applications. *J. Mater. Chem. B* **2020**, *8*, 9642−9651.

(3) Yang, X.; Zhang, D.; Ye, Y.; Zhao, Y. Recent Advances in Multifunctional Fluorescent Probes for Viscosity and Analytes. *Coord. Chem. Rev.* **2022**, *453*, No. 214336.

(4) Xiao, H.; Li, P.; Tang, B. Small Molecular Fluorescent Probes for Imaging of Viscosity in Living Biosystems. *Chem. − Eur. J.* **2021**, *27*, 6880−6898.

(5) Smith, M. M.; Chen, P. C. Y.; Li, C. S.; Ramanujam, S.; Cheung, A. T. W. Whole Blood Viscosity and Microvascular Abnormalities in Alzheimer's Disease. *Clin. Hemorheol. Microcirc.* **2009**, *41*, 229−239.

(6) Tamariz, L. J.; Young, J. H.; Pankow, J. S.; Yeh, H. C.; Schmidt, M. I.; Astor, B.; Brancati, F. L. Blood Viscosity and Hematocrit as Risk Factors for Type 2 Diabetes Mellitus: The Atherosclerosis Risk in Communities (ARIC) Study. *Am. J. Epidemiol.* **2008**, *168*, 1153−1160.

(7) Ciuffetti, G.; Schillaci, G.; Lombardini, R.; Pirro, M.; Vaudo, G.; Mannarino, E. Plasma Viscosity in Isolated Systolic Hypertension: The Role of Pulse Pressure. *Am. J. Hypertens.* **2005**, *18*, 1005−1008.

(8) Krzeszewski, M.; Gryko, D.; Gryko, D. T. The Tetraarylpyrrolo-[3,2-*b*]pyrroles-From Serendipitous Discovery to Promising Heterocyclic Optoelectronic Materials. *Acc. Chem. Res.* **2017**, *50*, 2334−2345.

(9) Janiga, A.; Glodkowska-Mrowka, E.; Stoklosa, T.; Gryko, D. T. Synthesis and Optical Properties of Tetraaryl-1,4-Dihydropyrrolo[3,2-*b*]pyrroles. *Asian J. Org. Chem.* **2013**, *2*, 411−415.

(10) Janiga, A.; Krzeszewski, M.; Gryko, D. T. Strongly Fluorescent Heterocycles and a Method for Their Synthesis, WO2014/070029A1, 2013.

(11) Krzeszewski, M.; Thorsted, B.; Brewer, J.; Gryko, D. T. Tetraaryl-, Pentaaryl-, and Hexaaryl-1,4-Dihydropyrrolo[3,2-*b*]-pyrroles: Synthesis and Optical Properties. *J. Org. Chem.* **2014**, *79*, 3119−3128.

(12) Tasior, M.; Vakuliuk, O.; Koga, D.; Koszarna, B.; Górski, K.; Grzybowski, M.; Kielesiński, Ł.; Krzeszewski, M.; Gryko, D. T. Method for the Large-Scale Synthesis of Multifunctional 1,4-Dihydropyrrolo[3,2-*b*]pyrroles. *J. Org. Chem.* **2020**, *85*, 13529−13543.

(13) Kubota, Y.; Koide, K.; Mizuno, Y.; Nakazawa, M.; Inuzuka, T.; Funabiki, K.; Sato, H.; Matsui, M. Synthesis and fluorescence properties of unsymmetrical 1,4-dihydropyrrolo[3,2-b]pyrrole dyes. *New J. Chem.* **2022**, *46*, 1533−1542.

(14) Ivanov, A. I.; Dereka, B.; Vauthey, E. A Simple Model of Solvent-Induced Symmetry-Breaking Charge Transfer in Excited Quadrupolar Molecules. *J. Chem. Phys.* **2017**, *146*, No. 164306.

(15) Friese, D. H.; Mikhaylov, A.; Krzeszewski, M.; Poronik, Y. M.; Rebane, A.; Ruud, K.; Gryko, D. T. Pyrrolo[3,2-*b*]pyrroles-From Unprecedented Solvatofluorochromism to Two-Photon Absorption. *Chem. − Eur. J.* **2015**, *21*, 18364−18374.

(16) Łukasiewicz, Ł. G.; Ryu, H. G.; Mikhaylov, A.; Azarias, C.; Banasiewicz, M.; Kozankiewicz, B.; Ahn, K. H.; Jacquemin, D.; Rebane, A.; Gryko, D. T. Symmetry Breaking in Pyrrolo[3,2-*b*]pyrroles: Synthesis, Solvatofluorochromism and Two-Photon Absorption. *Chem. − Asian J.* **2017**, *12*, 1736−1748.

(17) Dereka, B.; Rosspeintner, A.; Krzeszewski, M.; Gryko, D. T.; Vauthey, E. Symmetry-Breaking Charge Transfer and Hydrogen Bonding: Toward Asymmetrical Photochemistry. *Angew. Chem., Int. Ed.* **2016**, *55*, 15624−15628.

(18) Dereka, B.; Vauthey, E. Direct Local Solvent Probing by Transient Infrared Spectroscopy Reveals the Mechanism of Hydrogen-Bond Induced Nonradiative Deactivation. *Chem. Sci.* **2017**, *8*, 5057−5066.

(19) Bell, K.-J. J.; Kisiel, A. M.; Smith, E.; Tomlinson, A. L.; S Collier, G. S. Simple Synthesis of Conjugated Polymers Enabled via Pyrrolo[3,2-*b*]pyrroles. *Chem. Mater.* **2022**, *34*, 8729−8739.

(20) Zhao, B.; Xu, Y.; Liu, S.; Li, C.; Fu, N.; Wang, L. Non-Fullerene Receptor Material Based on Tetrarylpyrrole Nuclear and Its Application in Organic Solar Cell Device. CN108912125A, 2018.

(21) Domínguez, R.; Montcada, N. F.; de la Cruz, P.; Palomares, E.; Langa, F. Pyrrolo[3,2-*b*]pyrrole as the Central Core of the Electron Donor for Solution-Processed Organic Solar Cells. *ChemPlusChem* **2017**, *82*, 1096−1104.

(22) Zhou, Y.; Zhang, M.; Ye, J.; Liu, H.; Wang, K.; Yuan, Y.; Du, Y.-Q.; Zhang, C.; Zheng, C.-J.; Zhang, X.-H. Efficient Solution-Processed Red Organic Light-Emitting Diode Based on an Electron-Donating Building Block of Pyrrolo[3,2-*b*]pyrrole. *Org. Electron.* **2019**, *65*, 110−115.

(23) Wang, J.; Chai, Z.; Liu, S.; Fang, M.; Chang, K.; Han, M.; Hong, L.; Han, H.; Li, Q.; Li, Z. Organic Dyes Based on Tetraaryl-1,4-dihydropyrrolo[3,2-*b*]pyrroles for Photovoltaic and Photocatalysis Applications with the Suppressed Electron Recombination. *Chem. − Eur. J.* **2018**, *24*, 18032−18042.

(24) Canjeevaram Balasubramanyam, R. K.; Kumar, R.; Ippolito, S. J.; Bhargava, S. K.; Periasamy, S. R.; Narayan, R.; Basak, P. Quadrupolar (A-*π*-D-*π*-A) Tetra-Aryl 1,4-Dihydropyrrolo[3,2-*b*]-Pyrroles as Single Molecular Resistive Memory Devices: Substituent Triggered Amphoteric Redox Performance and Electrical Bistability. *J. Phys. Chem. C* **2016**, *120*, 11313−11323.

(25) Ji, Y.; Peng, Z.; Tong, B.; Shi, J.; Zhi, J.; Dong, Y. Polymorphism-Dependent Aggregation-Induced Emission of Pyrrolo-pyrrole-Based Derivative and Its Multi-Stimuli Response Behaviors. *Dyes Pigm.* **2017**, *139*, 664−671.

(26) Li, K.; Liu, Y.; Li, Y.; Feng, Q.; Hou, H.; Tang, B. Z. 2,5-Bis(4-alkoxycarbonylphenyl)-1,4-diaryl-1,4-dihydropyrrolo[3,2-*b*]pyrrole (AAPP) AIEgens: Tunable RIR and TICT Characteristics and Their Multifunctional Applications. *Chem. Sci.* **2017**, *8*, 7258−7267.

(27) Sadowski, B.; Hassanein, K.; Ventura, B.; Gryko, D. T. Tetraphenylethylenepyrrolo[3,2-*b*]pyrrole Hybrids as Solid-State Emitters: The Role of Substitution Pattern. *Org. Lett.* **2018**, *20*, 3183−3186.

(28) Ma, Y.; Zhang, Y.; Kong, L.; Yang, J. Mechanoresponsive Material of AIE-Active 1,4-Dihydropyrrolo[3,2-*b*]pyrrole Lumino-phores Bearing Tetraphenylethylene Group with Rewritable Data Storage. *Molecules* **2018**, *23*, 3255.

(29) Hawes, C. S.; Ó Máille, G. M.; Byrne, K.; Schmitt, W.; Gunnlaugsson, T. Tetraarylpyrrolo[3,2-*b*]pyrroles as Versatile and Responsive Fluorescent Linkers in Metal−Organic Frameworks. *Dalton Trans.* **2018**, *47*, 10080−10092.

(30) Janiga, A.; Krzeszewski, M.; Gryko, D. T. Diindolo[2,3-B:2′,3′-*f*]Pyrrolo[3,2-*b*]pyrroles as Electron-Rich, Ladder-Type Fluoro-phores: Synthesis and Optical Properties. *Chem. − Asian J.* **2015**, *10*, 212−218.

(31) Tasior, M.; Chotkowski, M.; Gryko, D. T. Extension of Pyrrolopyrrole π-System: Approach to Constructing Hexacyclic Nitrogen-Containing Aromatic Systems. *Org. Lett.* **2015**, *17*, 6106−6109.

(32) Tasior, M.; Czichy, M.; Łapkowski, M.; Gryko, D. T. Dibenzothienopyrrolo[3,2-b]pyrrole: The Missing Member of the Thienoacene Family. *Chem. − Asian J.* **2018**, *13*, 449−456.

(33) Tasior, M.; Gryko, D. T. Synthesis and Properties of Ladder-Type BN-Heteroacenes and Diazabenzoindoles Built on a Pyrrolo-pyrrole Scaffold. *J. Org. Chem.* **2016**, *81*, 6580−6586.

(34) Krzeszewski, M.; Kodama, T.; Espinoza, E. M.; Vullev, V. I.; Kubo, T.; Gryko, D. T. Nonplanar Butterfly-Shaped π-Expanded Pyrrolopyrroles. *Chem. − Eur. J.* **2016**, *22*, 16478−16488.

(35) Mishra, S.; Krzeszewski, M.; Pignedoli, C. A.; Ruffieux, P.; Fasel, R.; Gryko, D. T. On-Surface Synthesis of a Nitrogen-Embedded Buckybowl with Inverse Stone−Thrower−Wales Topology. *Nat. Commun.* **2018**, *9*, No. 1714.

(36) Wu, D.; Zheng, J.; Xu, C.; Kang, D.; Hong, W.; Duan, Z.; Mathey, F. Phosphindole Fused Pyrrolo[3,2-b]pyrroles: A New Single-Molecule Junction for Charge Transport. *Dalton Trans.* **2019**, *48*, 6347−6352.

(37) Tasior, M.; Kowalczyk, P.; Przybył, M.; Czichy, M.; Janasik, P.; Bousquet, M. H. E.; Łapkowski, M.; Rammo, M.; Rebane, A.; Jacquemin, D.; Gryko, D. T. Going Beyond the Borders: Pyrrolo[3,2-*b*]pyrroles with Deep Red Emission. *Chem. Sci.* **2021**, *12*, 15935−15946.

(38) Krzeszewski, M.; Dobrzycki, Ł.; Sobolewski, A. L.; Cyrański, M. K.; Gryko, D. T. Bowl-Shaped Pentagon- and Heptagon-Embedded Nanographene Containing a Central Pyrrolo[3,2-*b*]pyrrole Core. *Angew. Chem., Int. Ed.* **2021**, *60*, 14998−15005.

(39) Krzeszewski, M.; Dobrzycki, Ł.; Sobolewski, A. L.; Cyranski, M. K.; Gryko, D. T. Saddle-shaped Aza-nanographene with Multiple Odd-membered Rings. *Chem. Sci.* **2023**, *14*, 2353−2360.

(40) Poronik, Y. M.; Mazur, L. M.; Samoć, M.; Jacquemin, D.; Gryko, D. T. 2,5-Bis(azulenyl)pyrrolo[3,2-*b*]pyrroles − the Key Influence of the Linkage Position on the Linear and Non-linear Optical Properties. *J. Mater. Chem. C* **2017**, *5*, 2620−2628.

(41) Santra, M.; Jun, Y. W.; Bae, J.; Sarkar, S.; Choi, W.; Gryko, D. T.; Ahn, K. H. Water-Soluble Pyrrolo[3,2-*b*]pyrroles: Synthesis, Luminescence and Two-Photon Cellular Imaging Properties. *Asian J. Org. Chem.* **2017**, *6*, 278−281.

(42) Banasiewicz, M.; Stężycki, R.; Kumar, G. D.; Krzeszewski, M.; Tasior, M.; Koszarna, B.; Janiga, A.; Vakuliuk, O.; Sadowski, B.; Gryko, D. T.; Jacquemin, D. Electronic Communication in Pyrrolo-[3,2-*b*]pyrroles Possessing Sterically Hindered Aromatic Substituents. *Eur. J. Org. Chem.* **2019**, *2019*, 5247−5253.

(43) Guido, C. A.; Chrayteh, A.; Scalmani, G.; Mennucci, B.; Jacquemin, D. 'Simple Protocol for Capturing Both Linear-Response and State-Specific Effects in Excited-State Calculations with Continuum Solvation Models. *J. Chem. Theory Comput.* **2021**, *17*, 5155−5164.

(44) Loos, P. F.; Jacquemin, D. Evaluating 0−0 Energies with Theoretical Tools: A Short Review. *ChemPhotoChem* **2019**, *3*, 684−696.

(45) Tasior, M.; Koszarna, B.; Young, D. C.; Bernard, B.; Jacquemin, D.; Gryko, D.; Gryko, D. T. Fe(iii)-Catalyzed Synthesis of Pyrrolo[3,2-b]pyrroles: Formation of New Dyes and Photophysical Studies. *Org. Chem. Front.* **2019**, *6*, 2939−2948.